6. Blankenship, D. D., Bentley, C. R., Rooney, S. T. & Alley, R. B. Till beneath ice stream B.1. Properties derived from seismic travel times. *J. Geophys. Res.* **9,** 8903–8911 (1987).
7. Engelhardt, H., Humphrey, N., Kamb, B. & Fahnestock, M. Physical conditions at the base of a fast moving Antarctic ice stream. *Science* **248,** 57–59 (1990).
8. Engelhardt, H. & Kamb, B. Basal hydraulic system of a West Antarctic ice stream: constraints from borehole observations. *J. Glaciol.* **43,** 207–244 (1997).
9. Dalziel, I. W. D. & Elliot, D. G. West Antarctica: problem child of Gondwanaland. *Tectonics* **1,** 3–19 (1982).
10. Behrendt, J. C. *et al. The West Antarctic Rift System-A Review of Geophysical Investigations* 67–112 (Antarctic Res. Ser. 53, Am. Geophys. Union, Washington DC, 1991).
11. Cooper, A. K., Davey, F. J. & Hinz, K. in *Geological Evolution of Antarctica* (eds Thomson, M. R. A., Crame, J. A. & Thomson, J. W.) 285–292 (Cambridge Univ. Press, 1991).
12. Davey, F. J. *The Antarctic Continental Margin: Geology and Geophysics of the Western Ross Sea* 1–16 (Circum-Pacific Council for Energy and Resources, Houston, 1987).
13. Robertson, J. D., Bentley, C. R., Clough, J. W. & Greischar, L. L. in *Antarctic Geoscience* 1083–1090 (IUGS B4, Univ. Wisconsin Press, Madison, Wisconsin, 1982).
14. Rose, K. E. Characteristics of ice flow in Marie Byrd Land, Antarctica. *J. Glaciol.* **24,** 63–74 (1979).
15. Ten Brink, U. S., Bannister, S., Beaudoin, B. C. & Stern, T. A. Geophysical investigations of the tectonic boundary between East and West Antarctica. *Science* **261,** 45–50 (1993).
16. Rooney, S. T., Blankenship, D. D., Bentley, C. R. & Alley, R. B. Till beneath ice stream B.2. Structure and continuity. *J. Geophys. Res.* **9(B9),** 8913–8920 (1987).
17. Retzlaff, R., Lord, N. & Bentley, C. R. Airborne-radar studies: Ice streams A, B and C, West Antarctica. *J. Glaciol.* **39(133),** 495–506 (1993).
18. Hodge, S. M. & Doppelhammer, S. Onset of streaming flow of ice streams. *J. Geophys. Res.* **101,** 6669–6677 (1996).
19. Scambos, T. A. & Bindshadler, R. A. Ice flow at the confluence of two ice stream tributaries revealed by sequential satellite imagery. *Ann. Glaciol.* **17,** 177–182 (1993).
20. Bindschadler, R. A. & Vornberger, P. L. AVHRR imagery reveals Antarctic ice dynamics. *Eos* **71,** 741–742 (1990).
21. Anandakrishnan, S., Blankenship, D. D., Alley, R. B. & Stoffa, P. L. Influence of subglacial geology on the position of a West Antarctic ice stream from seismic observations. *Nature* **394,** 62–65 (1998).
22. Shabtaie, S. & Bentley, C. R. Ice-thickness map of the West Antarctic ice streams by radar sounding. *Ann. Glaciol.* **11,** 126–135 (1988).
23. Drewry, D. J. *Antarctica: Glaciological and Geophysical Folio* (Cambridge Univ. Press, 1983).
24. Shabtaie, S. & Bentley, C. R. West Antarctic ice streams draining into the Ross ice shelf: configuration and mass balance. *J. Geophys. Res.* **92(B2),** 1311–1336 (1987).
25. Anandakrishnan, S. & Alley, R. B. Stagnation of ice stream C, West Antarctica by water piracy. *Geophys. Res. Lett.* **24,** 265–268 (1997).
26. Brozena, J. M. *et al.* CASERTZ 91-92: Airborne gravity and surface topography measurements. *Antarc. J. US* **28,** 1–3 (1993).
27. Behrendt, J. C. *et al.* CASERTZ aeromagnetic data reveal late Cenozoic flood basalts in the West Antarctic rift system. *Geology* **22,** 527–530 (1994).

Acknowledgements. We thank R. Arko, M. Studinger and S. Kempf for assistance. This Letter was improved by contributions from G. Karner and C. Small. This work was supported by the US NSF.

Correspondence and requests for materials should be addressed to R.E.B. (robinb@ldeo.columbia.edu).

Influence of subglacial geology on the position of a West Antarctic ice stream from seismic observations

S. Anandakrishnan*, D. D. Blankenship†, R. B. Alley* & P. L. Stoffa†

* *Earth System Science Center and Department of Geosciences, Pennsylvania State University, University Park, Pennsylvania 16802, USA*
† *Institute for Geophysics, University of Texas–Austin, Austin, Texas 78759, USA*

Ice streams drain much of the interior West Antarctic Ice Sheet and buffer the main ice reservoir from oceanic influences[1,2]. The slow-flowing interior feeds the floating Ross Ice Shelf with ice via fast-flowing ice streams[3] that are believed to modulate sea-level change through their control of inland ice storage. Understanding ice-stream behaviour, and predicting the response to climate change[4], requires a better knowledge of the subglacial geology[5,6]. It is known that a thawed ice-bed and high-pressure basal water are necessary, but not sufficient, conditions to cause ice streaming[7,8]. Moreover, it has been hypothesized that a soft sedimentary bed is also required, because of its intrinsic low frictional resistance to flow[9], and owing to its high erodibility so as to generate till that can deform and lubricate ice motion[10,11], or to bury rough features and smooth the bed for sliding. Here we use seismic observations to provide evidence that one margin of the upglacier part of an ice stream is directly above the boundary of a basin with such sedimentary fill. The ice stream is within the basin and the ice outside the basin is slow-flowing. The basin fill presents an order-of-magnitude lower frictional resistance to ice flow than the subglacial material outside the basin. We conclude that the ice stream position is dependent on subglacial geology.

We identify the ice stream margin by the striking increase in flow velocity from ~10 m yr^{-1} to over 60 m yr^{-1} over a distance of 4.5 km (between Km 52.5 and Km 57 of Fig. 1; the Km numbers refer to distance in kilometres from the beginning of our line at Km0) that is correlative with flow-bands in satellite imagery[12,13]. The ice flow velocities (Fig. 1b) as well as the surface elevation were determined by repeat GPS (Global Positioning System) surveying with a one-year interval between surveys. A combined reflection and refraction seismic profile along the GPS profile crossed the boundary between the slow-flowing interior ice of the West Antarctic Ice Sheet and the fast-moving ice-stream ice (Fig. 1a). The seismic data were acquired in the 1994–95 austral summer by using a towed snow-streamer with 14 Hz geophones every 25 m from 0 to 10.5 km distance from the source. The shot interval was 300 m and the line was directed east–west with higher shotpoint numbers (SP) to the west.

Common-shot gathers were collected every 300 m along the line, and the times of first arrival for the direct wave t_d and the subglacially refracted wave t_r were picked (Fig. 2 is a representative gather at location SP = Km 51.0). To interpret these data we first formed a model of the ice and subglacial structure beneath the line and then performed a least-squares inversion to determine model

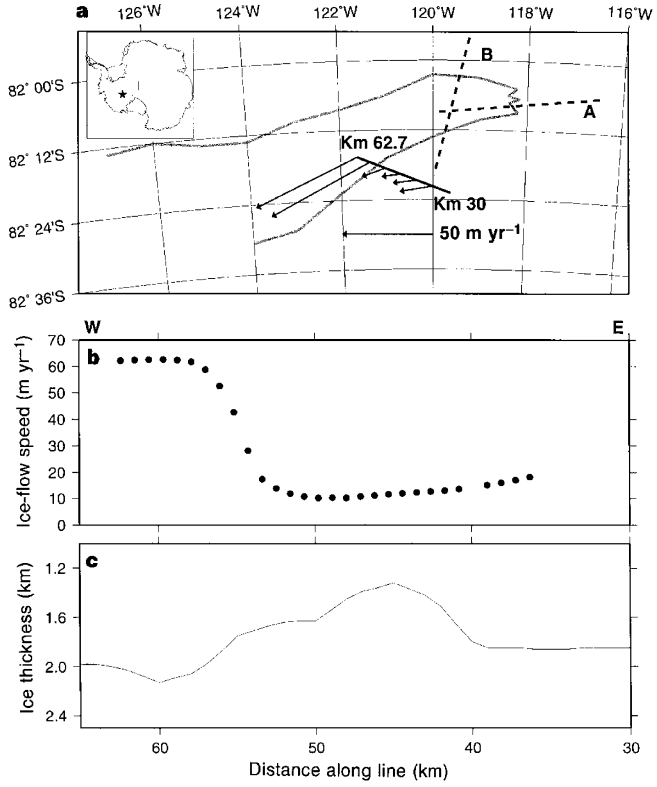

Figure 1 Location map showing the ice stream boundaries and the experiment profile line, together with ice flow speeds and ice thickness along that line. **a**, Map showing the seismic line (solid line) and selected ice flow vectors along the line (determined by repeat GPS measurements; see text). All the measured ice flow speeds are plotted in **b**. The grey curves are the boundaries and onset of ice stream C as identified by Hodge and Doppelhammer[12] (these were digitized from their Fig. 5). The two dashed lines are profiles A and B of Bell *et al.*[13] (included here for reference). The inset is a map of Antarctica with a star marking our study-area. The + symbol indicates the position of the South Pole. **b**, Ice flow speeds (m yr^{-1}); the abscissa is the position along the seismic line in kilometres; **c**, ice thickness in km.

parameters that minimized the misfit between the modelled and measured refracted-wave arrival times.

The ice-column thickness along the line was determined by creating a 'zero-offset stack section' from the ice-bottom reflection data[14]. The ice-bottom reflection travel-times were converted to ice thickness by using a four-layer firn seismic-velocity model and an ice-column compressional-wave (p-wave) velocity of $v_I = 3{,}831 \pm 10\,\mathrm{m\,s^{-1}}$, both determined by high-resolution (receiver spacing of 1 m) refraction shooting (at Km 30) as in ref. 15. Because of strain-enhanced densification, average densities in the firn layer (and the firn p-wave velocities) could differ by up to ~20% between the ice sheet and the ice stream (with ice-stream firn denser than ice-sheet firn at the same depths)[16]. This error and the uncertainty in ice velocity resulted in ice thickness determinations accurate to 15 m (Fig. 1c).

We modelled the refracted arrival travel times through our hypothesized subglacial structures by two-dimensional ray tracing[17]. The arrival times are functions of shotpoint SP and offset $\Delta : t_r = t_r(\mathrm{SP}, \Delta)$. The misfit between the modelled (t_{mod}) and measured refracted arrivals, $\delta(\mathrm{SP}, \Delta) = t_{mod} - t_r$, the r.m.s. misfit $\langle\delta\rangle$, the χ^2 value, and the goodness-of-fit q (ref. 18) were used to evaluate the models.

Initially we calculated residuals for a model of ice over a constant-velocity layer (hereafter the refracting layer is called basement). The model of ice over basement did not fit the data well (Fig. 3a). The misfit was caused by a delay in the measured t_r arrival times relative to the model (Fig. 3a). A prominent feature was a rapid increase in the absolute value of $\langle\delta\rangle$ to the west of SP = Km 56.7, marked by L, where the data were increasingly delayed relative to the model. West of SP = Km 59.7, the delay had become so large that the high-amplitude direct wave t_d arrived first and masked the refracted arrival t_r.

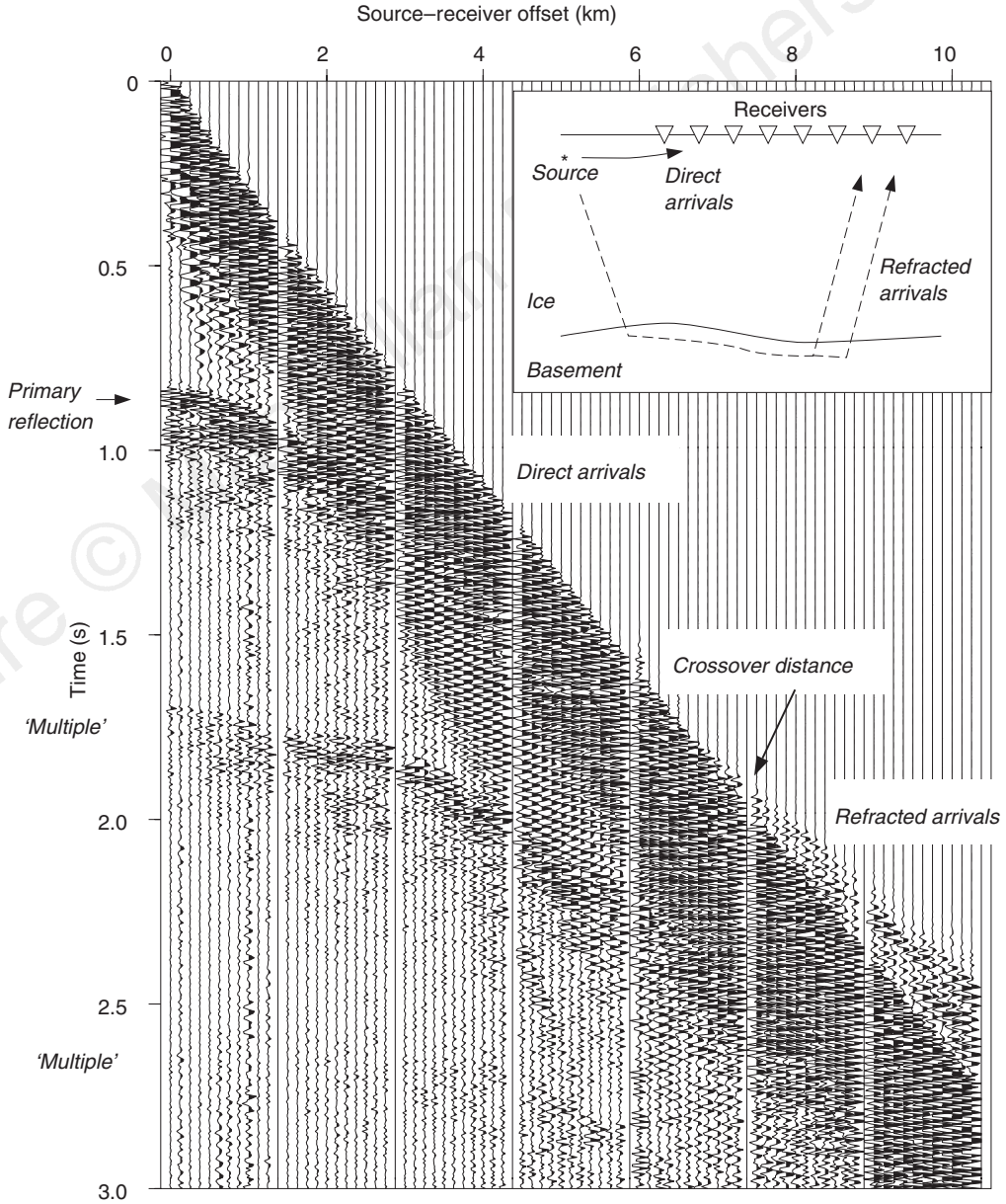

Figure 2 Common shot gather for a shot at SP = Km 51.0. Each vertical trace represents the acoustic energy arriving at that offset Δ; the data were sampled at 1 ms resolution (for clarity, only every fifth trace is shown). The first prominent arrival at near-offsets is the 'direct arrival' (t_d) of energy that travels along the surface of the ice sheet. The break in slope of the first arrivals is at the 'crossover distance' $\Delta_c = 6.5$ km; the first arrivals at larger offsets are from energy that has refracted along a high-seismic-velocity basement layer beneath the ice[14]. Because of the ~40° incidence angle of the raypaths, there is ~1.5 km horizontal offset between a surface site and the corresponding illumination site at the bed. The arrival marked 'primary reflection' is the energy reflected from the bed of the ice. The inset is a diagram representing the direct and refracted energy paths.

We attempted to reduce the residuals by constructing two alternative models: one, model (1), in which refracted arrivals travel along the top of the basement, which is directly in contact with the ice, and the arrival-time delays are caused by lateral variations in seismic velocity of the basement, and the other, model (2), in which the refracted arrivals travel along the top of a fixed-velocity basement, but the delays are caused by varying thicknesses of lower-velocity sediments interposed between the ice and basement. We used a least-squares inversion[19] to solve for the model parameters that resulted in the best fit between t_r and t_{mod} for each of the models. Model (1), where the inversion parameter is the basement velocity, $v_B(x)$, did not significantly improve the fit (minimum r.m.s.d. misfit $\langle\delta\rangle = 21$ ms, $\chi^2 = 6{,}700$, and an infinitesimal q); the v_B are well resolved, but the misfit is because of the incorrect apparent velocities of the refracted arrivals.

In model (2), the parameters are the thicknesses of the low-velocity layer $H(x)$ along the line, with the seismic velocities of both the basement and of the low-velocity layer fixed. We fixed the basement velocity at $v_B = 5.7\,\mathrm{km\,s^{-1}}$, determined from a fully reversed refraction experiment between Km 42 and Km 54. This velocity is consistent with a large-offset refraction study that was conducted 30–200 km from our experiment[20]. We introduce a layer L, of p-wave velocity v_L and thickness $H(x)$, between the ice and the basement. We place an upper bound of $v_L = 4.9\,\mathrm{km\,s^{-1}}$; for $v_L > 4.9\,\mathrm{km\,s^{-1}}$, energy refracted along the top of layer L would have been observed arriving before the direct arrival, but this is not observed. A reasonable lower bound for non-dilatant sediments in central West Antarctica is $v_L = 2\,\mathrm{km\,s^{-1}}$ (ref. 21). The layer p-wave velocity, v_L, was fixed at $2\,\mathrm{km\,s^{-1}} \le v_L \le 4.9\,\mathrm{km\,s^{-1}}$ and the inversion for $H(x)$ is conducted. This process was repeated for a number of v_L in this range.

The best-fit inversions yield the residuals shown in Fig. 3b and c for $v_L = 2\,\mathrm{km\,s^{-1}}$ and $v_L = 4.9\,\mathrm{km\,s^{-1}}$, respectively. The layer thicknesses are well resolved along the line with better than 90% confidence between Km 30 and Km 55, and better than 68% confidence between Km 55 and Km 59. An F-test for significantly different variances finds that the model with $v_L = 2.0\,\mathrm{km\,s^{-1}}$ has a lower variance at the 68% significance level. Whatever the value of v_L, a thick basin must be introduced to the west of Km 51 (Fig. 4). For $x > 58$ km, H must be greater than 400 m (the basin thickness at $x = 58$ km) because of the absence of refracted arrivals for SP > Km 59.7.

Modelling of ice stream margins[22] shows that when the bed friction changes abruptly from high to low friction by an order of magnitude or more, the entire margin (zone of rapid velocity change) is located on the low-friction side; for small changes in bed friction (a factor of two), the margin straddles the change and is symmetrical across the boundary. On the basis of the velocity profile

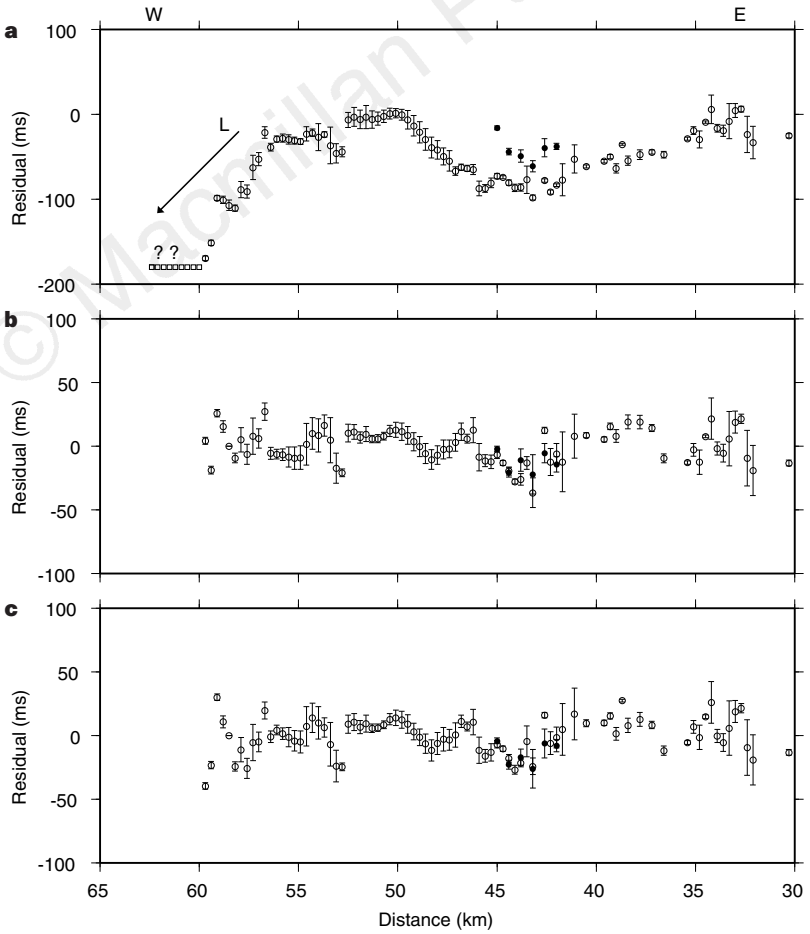

Figure 3 Mean residuals $\langle\delta(\mathrm{SP}, \Delta)\rangle = t_{mod} - t_r$ between the model and the data are plotted at the shotpoint (SP). The error bars indicate one standard deviation. The filled circles are for 'reversed' shots where the receivers were to the west of the source; all other data were recorded with receivers to the east of the source. The open boxes (with the question marks) indicate locations where data were collected but no pre-direct-wave refracted arrivals were observed (the signal-to-noise ratios were high, so refracted arrivals would have been observed if they had been present). **a**, Residuals for a model of ice over basement as in Fig. 4, but with no sediments. Number of data points $N = 6{,}195$, r.m.s. misfit $\langle\delta\rangle = 52$ ms, $\chi^2 = 1.7 \times 10^5$, and infinitesimal q. Basement velocity is $v_B = 5.7\,\mathrm{km\,s^{-1}}$. The squares at SP = Km 59.7 and higher indicate shotpoint locations where the crossover distance was greater than the maximum offset of the recording array. **b**, As in **a**, but for ice over a sedimentary basin of $v_L = 2.0\,\mathrm{km\,s^{-1}}$. r.m.s. misfit $\langle\delta\rangle = 14.9$ ms, $\chi^2 = 6{,}119$ and $q = 0.47$. **c**, As in **b**, but with $v_L = 4.9\,\mathrm{km\,s^{-1}}$ and $\langle\delta\rangle = 15.1$ ms, $\chi^2 = 6{,}174$ and $q = 0.2$ (the models are shown in Fig. 4).

as well as the position of the shear margin relative to the basin boundary, we interpret the slip-friction change as at least a factor of ten[22].

The ice thickness h increases by 20% across the margin into the ice stream, but the surface slope α decreases by 30% (with lower surface slopes on the ice stream) (ref. 13). Thus, the driving stress τ is lower for the fast-moving ice stream ($\tau = \rho g h \alpha$, where $\rho = 917\,\mathrm{kg\,m^{-3}}$ is the density of ice, $g = 9.8\,\mathrm{m\,s^{-2}}$ is the gravitational acceleration, α is the surface slope and h is the ice thickness[23]). We discount a frozen bed as the cause of the slow-moving ice. The bed will be thawed if the heat flow at the bed Q (including both geothermal heat Q_{geo} and heat of sliding and heat of deformation $Q_{ice} = \tau \times u$, where u is the ice-flow speed) is high enough to maintain a bed temperature $T_B = -1.4\,^{\circ}\mathrm{C}$ (the pressure-melting point for an ice-column thickness $h = 1{,}700\,\mathrm{m}$, the average ice-thickness of the slow-moving ice). Using the steady-state solution due to Robin[24], with accumulation rate $b = 0.14\,\mathrm{m\,yr^{-1}}$ and surface temperature $T_S = -27\,^{\circ}\mathrm{C}$ (ref. 25), we find that for any geothermal heat flow $Q_{geo} > 35\,\mathrm{mW\,m^{-2}}$, the bed will be thawed beneath our entire profile. Geothermal heat flow as low as that is unlikely in the West Antarctic; values twice as great are more likely[5,16,26]. We justify using a steady-state calculation by noting that the regions upflow of our line are not grossly unsteady[27], although more work is needed. In addition, we justify *a posteriori* the conclusion that there is a thawed bed by noting that our calculation must be in error by a factor of two to negate that conclusion.

Nearly identical locations for the marked increase in ice flow speeds (at Km 52.5) and the boundary of the low-seismic-velocity subglacial basin (at Km 51) are unlikely to be a coincidence. We conclude that the low-seismic-velocity material presents a low frictional resistance to flow, and consists of easily erodible sediments similar to those that have been observed beneath ice stream B ($v_L = 2.0$–$2.3\,\mathrm{km\,s^{-1}}$)[28]; the basin has a strong negative magnetic anomaly[13,29], also indicative of sediments. We further suggest that these sediments are necessary to maintain rapid ice-stream flow in the upper reaches of the ice stream. The ice does not stream over the thinner, narrower low-seismic-velocity materials near Km 40 because, as demonstrated in ref. 22, narrow ice streams would be dominated by side shear, which would not permit the large velocities characteristic of streaming flow. For a potential ice stream three to four ice thicknesses wide, a decrease in basal shear stress from the driving stress τ to zero through the introduction of perfect lubrication would raise the side shear stress only to 2τ averaged over the ice thickness, producing little change in the ice velocity in the lubricated region. Finally, a large positive gravity anomaly 10–20 km upflow of this region[13,30] suggests that the thinner layer at Km 40 might pinch out upflow, further decreasing the likelihood of streaming.

The ice flows slowly (10–$15\,\mathrm{m\,yr^{-1}}$) where sediments are intermittent. To the west of Km 51 up to the end of the line at Km 63, the low-velocity layer thickens continuously. The ice above these sediments is characteristic of ice-stream ice with higher flow-speeds (60–$70\,\mathrm{m\,yr^{-1}}$), a distinct margin visible in satellite imagery, and a rapid increase in flow speed across this margin. The velocity gradient across the margin is steep, and the margin is entirely contained within the sedimentary basin, suggesting a bed with low frictional resistance within the basin. The model that best fits the data is of a 400–600-m-thick basin of $v_L = 2.0$–$2.3\,\mathrm{km\,s^{-1}}$ sediments (Fig. 4). We conclude that the configuration of the ice streams, and projections about the future of the West Antarctic Ice Sheet (which is intimately tied to the ice streams) can be understood only in the context of the subglacial geology and, in particular, the distribution, thickness, and composition of sedimentary basins, all of which are poorly known. □

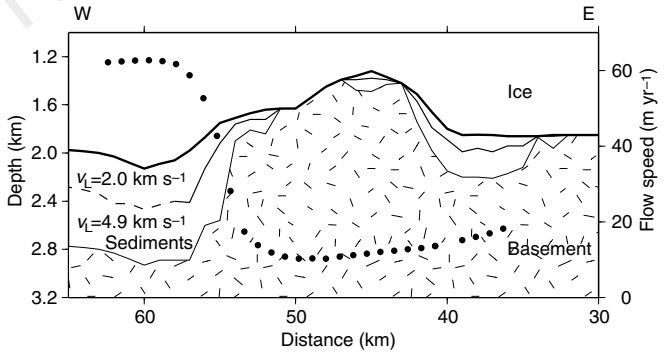

Figure 4 The final models from the ice/sediment/basement model-inversions. The ice thickness (top curve) is determined by seismic-reflection processing. The sediment layer thickness is determined by seismic-refraction processing. The layer depths for an assumed $v_L = 2.0\,\mathrm{km\,s^{-1}}$ model (centre curve) and an assumed $v_L = 4.9\,\mathrm{km\,s^{-1}}$ (bottom curve) are shown. To the west of Km 58 we fix the sediment thickness to the thickness value at Km 58 and indicate that with dashed lines; as discussed in the text, the sediments there are at least that thick. For reference, the ice-flow velocities along the line are superimposed, with the flow-speed axis on the right-hand side (see Fig. 1b).

Received 5 March 1997; accepted 10 March 1998.

1. Hughes, T. J. The West Antarctic Ice Sheet: instability, disintegration, and initiation of ice ages. *Rev. Geophys.* **13,** 502–526 (1975).
2. Mercer, J. H. West Antarctic ice sheet and CO_2 greenhouse effect: a threat of disaster. *Nature* **271,** 321–325 (1978).
3. Rose, K. Characteristics of ice flow in Marie Byrd Land, Antarctica. *J. Glaciol.* **24,** 63–74 (1979).
4. Anandakrishnan, S. & Alley, R. B. Stagnation of ice stream C, West Antarctica by water piracy. *Geophys. Res. Lett.* **24**(3), 265–268 (1997).
5. Blankenship, D. D. *et al.* Active volcanism beneath the West Antarctic ice sheet and implications for ice-sheet stability. *Nature* **361,** 526–529 (1993).
6. Boulton, G. S. Theory of glacial erosion, transport and deposition as a consequence of sub-glacial sediment deformation. *J. Glaciol.* **42**(140), 43–62 (1996).
7. Anandakrishnan, S. & Alley, R. B. Ice stream C, Antarctica, sticky-spots detected by micro-earthquake monitoring. *Ann. Glaciol.* **20,** 183–186 (1994).
8. Alley, R. B., Anandakrishnan, S., Bentley, C. R. & Lord, N. A water-piracy hypothesis for the stagnation of ice stream C, Antarctica. *Ann. Glaciol.* **20,** 187–194 (1994).
9. Boulton, G. S. & Jones, A. S. Stability of temperate ice caps and ice sheets resting on beds of deformable sediment. *J. Glaciol.* **24**(90), 29–43 (1979).
10. Blankenship, D. D., Bentley, C. R., Rooney, S. T. & Alley, R. B. Seismic measurements reveal a saturated, porous layer beneath an active Antarctic ice stream. *Nature* **322,** 54–57 (1986).
11. Alley, R. B., Blankenship, D. D., Bentley, C. R. & Rooney, S. T. Deformation of till beneath ice stream B, West Antarctica. *Nature* **322,** 57–59 (1986).
12. Hodge, S. M. & Doppelhammer, S. K. Satellite imagery of the onset of streaming flow of ice streams C and D, West Antarctica. *J. Geophys. Res.* **101**(C3), 6669–6677 (1996).
13. Bell, R. E. *et al.* Influence of subglacial geology on the onset of a West Antarctic ice stream from aerogeophysical observations. *Nature* **394,** 58–62 (1998).
14. Telford, W. M., Geldart, L. P., Sheriff, R. E. & Keys, D. A. *Applied Geophysics* (Cambridge Univ. Press, 1976).
15. Anandakrishnan, S., Blankenship, D. D., Alley, R. B. & Bentley, C. R. Density–depth profile determined by seismic-refraction studies: ice stream B, West Antarctica. *Ann. Glaciol.* **11,** 198 (1988).
16. Alley, R. B. & Bentley, C. R. Ice-core analysis on the Siple Coast of West Antarctica. *Ann. Glaciol.* **11,** 1–7 (1988).
17. Zelt, C. A. & Ellis, R. M. Practical and efficient ray tracing in two-dimensional media for rapid traveltime and amplitude forward modeling. *Can. J. Exp. Geophys.* **24,** 16–31 (1988).
18. Press, W. H., Flannery, B. P., Teukolsky, S. A. & Vetterling, W. T. *Numerical Recipes in C. The Art of Scientific Computing* (Cambridge Univ. Press, 1988).
19. Zelt, C. A. & Smith, R. B. Seismic traveltime inversion for a 2-D crustal velocity structure. *Geophys. J. Int.* **108**(1), 16–34 (1992).
20. Clarke, T. S., Burkholder, P. D., Smithson, S. B. & Bentley, C. R. in *The Antarctic Region: Geological Evolution and Processes* 485–493 (Terra Antarctica Publication, Siena, Italy, 1997).
21. Rooney, S. T., Blankenship, D. D., Alley, R. B. & Bentley, C. R. Till beneath ice stream B. 2. Structure and continuity. *J. Geophys. Res.* **92**(B9), 8913–8920 (1987).
22. Raymond, C. F. Shear margins in glaciers and ice sheets. *J. Glaciol.* **42**(140), 90–102 (1996).
23. Paterson, W. S. B. *The Physics of Glaciers* 2nd edn (Pergamon, Oxford, 1981).
24. Robin, G. deQ. Ice movement and temperature distribution in glaciers and ice sheets. *J. Glaciol.* **2,** 523–532 (1955).
25. Whillans, I. M. & Bindschadler, R. A. Mass balance of ice stream B, West Antarctica. *Ann. Glaciol.* **11,** 187–193 (1988).
26. Sclater, J. G., Jaupart, C. & Galson, D. The heat flow through oceanic and continental crust and the heat loss of the Earth. *Rev. Geophys. Space Phys.* **18,** 269–311 (1980).
27. Whillans, I. M. in *The Climatic Record in Polar Ice sheets, a Study of Isotopic and Temperature Profiles in Polar Ice Sheets* (ed. Robin, G. de Q.) 70–76 (Cambridge Univ. Press, 1983).
28. Rooney, S. T., Blankenship, D. D., Alley, R. B. & Bentley, C. R. in Seismic reflection profiling of a sediment-filled graben beneath ice stream B, West Antarctica. *Geological Evolution of Antarctica* (eds Thomson, M. R. A., Crame, J. A. & Thomson, J. W.) 261–265 (Cambridge Univ. Press, 1991).
29. Behrendt, J. C. *et al.* CASERTZ aeromagnetic data reveal late Cenozoic flood basalts (?) in the West Antarctic rift system. *Geology* **22,** 527–530 (1994).
30. Brozena, J. M. *et al.* CASERTZ 1991 and 1992: gravity and surface topography. *Antarct. J. US* **10,** 1–3 (1993).

Acknowledgements. We thank A. M. Smith, the British Antarctic Survey, S. Saustrup, UNAVCO, ASA, VXE-6, Fjord Instruments, and Landmark Graphics for assistance. We thank the US National Science Foundation for financial support.

Correspondence and requests for materials should be addressed to S.A. (e-mail: sak@essc.psu.edu).